Multiarm star polymers dynamics

2001 J. Phys.: Condens. Matter 13 R855

(http://iopscience.iop.org/0953-8984/13/41/202)

INSTITUTE OF PHYSICS PUBLISHING JOURNAL OF PHYSICS: CONDENSED MATTER

J. Phys.: Condens. Matter **13** (2001) R855–R876 PII: S0953-8984(01)19758-4

TOPICAL REVIEW

Multiarm star polymers dynamics

Dimitris Vlassopoulos[1], George Fytas[1], Tadeusz Pakula[2] and Jacques Roovers[3]

[1] Foundation for Research and Technology–Hellas (FORTH), Institute of Electronic Structure and Laser, 71110 Heraklion, Crete, Greece
[2] Max-Planck Institut für Polymerforschung, D-55021 Mainz, Germany
[3] National Research Council, Institute for Environmental Chemistry and Chemical Technology, Ottawa, Ontario, Canada K1A 0R6

Received 5 June 2001
Published 28 September 2001
Online at stacks.iop.org/JPhysCM/13/R855

Abstract

Multiarm star polymers, consisting of a high number of linear homopolymer arms joined covalently to a central core, represent model soft 'hybrid' spheres encompassing both polymeric (arm) and colloidal (core) character. Due to this topology, the single star has a nonuniform monomer density distribution. In nondilute solutions, a liquid-like ordering occurs as a consequence of the enhanced osmotic pressure that outbalances the entropic stretching of the arms; this type of order persists in the melt as well, due to 'macromolecular excluded volume' effects. The resulting rich dynamic response, which is presented in this review, exhibits signatures of both polymeric and colloidal behaviour. In solution, concentration and number density fluctuations relax via cooperative diffusion, self-diffusion and structural relaxation. In the melt, the viscoelastic terminal relaxation involves arm relaxation (independent of arm number) and structural rearrangements of the stars (strongly dependent on arm number and size). The identification of the relaxation mechanisms in such complex soft spheres provides the necessary ingredients for the molecular design and control of novel composite materials combining properties of polymers and colloids.

1. Introduction

The efficient design of new mesoscopic materials with desired properties intermediate between different classes of soft systems represents one of the most formidable challenges in soft condensed matter physics [1–5]. Linear polymers and colloids represent two of the most studied classes of soft materials because of their interesting properties and widespread applicability [6, 7]. They also constitute the extremes in a spatial organization of a large number of low molecular units, in the former case linear flexible strings and in the latter case a stiff compact assembly with a well-defined shape (e.g. spherical). This architectural difference involves considerable differences in the dynamics and consequently in the properties of these

systems. For example, semidilute solutions (at concentration c above the overlap concentration c^*) of homopolymers (a contiguous sequence of N monomers covalently bonded) exhibit collective concentration fluctuations which are controlled by the osmotic pressure of the system [8, 9]. This reflects weak interactions at monomeric scales, of $O(k_BT)$ or less, with a relevant correlation length ξ_c of O(nm) independent of N; very high concentrations are therefore needed for short range ordering, if attainable at all. On the other hand, colloidal dispersions of solid particles with radius R_0 in a host fluid exhibit a size-dependent dynamic behaviour governed by collective thermal number density fluctuations, with correlation length $O(R_0)$, and the ordering occurs at relatively low number densities and is long range [10, 11]. The intermediate behaviour between short-range polymeric and long-range colloidal interactions remains a rich area of research because of the great potential to combine polymeric with colloidal mesoscopic characteristics. One way of achieving such a performance is by constructing macromolecular objects of more complex architecture. A great deal of research effort was recently invested in this direction. In particular, in addition to the well-studied diblock copolymer micelles [12–22], Leibler and co-workers investigated the dynamics of polyelectrolyte microgels and found them to behave as colloidal particles with tunable interaction potential [23, 24]. In addition, hard spherical particles with chemically grafted polymeric chains (arms) represent another colloidal system with controlled softness; typical examples include polymeric latex spheres with arms of varying sizes and grafting density [17, 25–28], which can also form networks around the spheres and respond to temperature via swelling [29]. Multiarm star polymers represent another promising system for varying the softness [30–33].

In this paper, we review the *linear* dynamic properties of multiarm star polymers with emphasis on their interplay with their structure, as well as the identification of the contributing relaxation processes, both in solution and in the melt.

Recent advances in macromolecular chemistry have led to the anionic synthesis of nearly monodisperse model star homopolymers with high functionality f (up to 128 branches) [30, 31, 34, 35]. Owing to their topology, these stars exhibit a nonuniform monomer density distribution, as explained rigorously by Daoud and Cotton [36] (as well as the subsequent relevant theoretical work by Zhulina and co-workers [37, 38] and its extension to account for neutral and charged brushes formed by micelles or grafted colloidal spheres [39]) and verified with computer simulations [35, 40, 41], as well as experimentally [42]. An identical nonuniform monomer density distribution was also studied for the case of block copolymer micelles [19, 20, 22]. As such, they can be thought of as ideal inherently stable particles exhibiting a core–corona morphology with two characteristic length scales: small, ξ_c, which represents the size of a self-avoiding segment (interaction blob), and is of polymeric nature, and large, R_0, which represents typically the overall radius of the star, and is of colloidal nature. Figure 1(a) depicts a cartoon representation of a multiarm star along with a simulated structure of a 64-arm star obtained from an equilibrated melt [40]. Figure 1(b) depicts the simulated monomer density profile for single stars of different functionality in the melt state [40]. This figure implies that near the centre of a given star, segments belonging to different neighbouring stars are present, i.e. interpenetration increases with decreasing f. The inset of figure 1(b) depicts the dependence of the radius of the star core in the melt on the arm functionality for different arm sizes. Two regions can be distinguished: that for stars with $f < 24$ and the region with distinct impenetrable core [36, 40, 43] for higher f values.

Molecularly dispersed in a good solvent, such hyperstars exhibit liquid-like order as soon as their concentration exceeds c^*, as demonstrated by SANS and SAXS experiments [44–47]. The reason for their liquid-like structure formation is the enhanced osmotic pressure which outbalances the elastic energy of the entropically stretched arms [48, 49]. Such topologically complex materials with 'intermediate' properties are expected to exhibit a rich dynamics

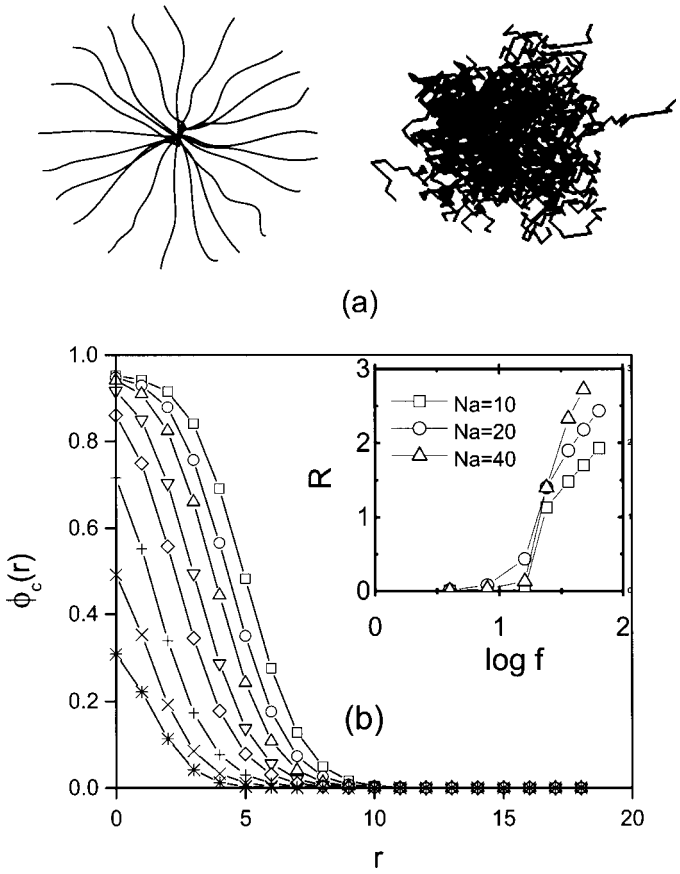

Figure 1. (a) Cartoon representation of a multiarm star polymer (left) and the simulated structure of a 64-arm star with $N_a = 20$, taken from an equilibrated melt (right). (b) Simulated monomer density profile of a single star polymer with $N_a = 20$ and varying functionality, in terms of intrastar monomer density, $\phi_c(r)$, against distance from centre, r ($*$, $f = 2$; $\times$, $f = 4$; $+$, $f = 8$; $\diamond$, $f = 16$; ∇, $f = 24$; Δ, $f = 36$; $\bigcirc$, $f = 48$; $\square$, $f = 64$. Inset: simulated star core radius R as a function of f for different N_a values.

characterized by multiple relaxation mechanisms [32, 35, 50], in contrast to the simpler behaviour of their two extremes, i.e. polymers and colloids. We show here that the presence of both length scales in these systems is responsible for their dynamic response, which is characterized by a combination of polymeric and colloidal motions.

2. Molecular features of the model multiarm star polymers

A series of regular multiarm 1, 4-polybutadiene stars was synthesized by Roovers and co-workers using chlorosilane chemistry, yielding central dendritic cores of spherical shape and different generations on which the desired number of polymeric arms were grafted [30, 31, 34]; the resulting stars ranged in functionality, f, from 18 to 128 and nominal arm molecular weight from 5000 to 80 000 (all above the entanglement molecular weight of polybutadiene).

Table 1. Molecular characteristics of of the 1, 4-polybutadiene stars [30, 32, 34, 51].

Code	f	$M_w \times 10^6$ (g mol)$^{-1}$	ε[a]	N_a[b]	T_g (°C)	R_g (nm)[c]
PB165	2	0.165	—	1528	−96	18
4S40	4	0.159	0	736	−96	16
4S120	4	0.375	0	1732	−96	26
1518	18	0.311	0	320	−92	12.4
2518	19	0.541	0.056	555	−92	17.4
3718	18	0.762	0	782	−92	19.9
3210	31	0.301	0.031	174	−92	10
3216	32	0.558	0	322	−92	13.4
3220	33	0.644	0.031	372	−92	14.5
3237	35	1.33	0.094	768	−92	22.4
3280	34	3.01	0.063	1738	−92	37.6
6407	62	0.395	0.031	117	−92	9.8
6415	60	0.725	0.062	224	−92	12.7
6430	56	1.34	0.125	443	−92	18.5
6460	61	2.89	0.047	880	−92	28
12 807	124	0.84	0.031	126	−92	10.5
12 814	125	1.62	0.023	241	−92	15.8
12 828	114	2.98	0.078	483	−92	21.6
12 856	127	5.95	0.008	870	−92	34.5
12 880	122	8.8	0.047	1333	−92	42.4

[a] Functionality polydispersity, estimated as $\varepsilon = |f_n - f|/f$ where f_n is the nominal functionality and f the tabulated measured one.
[b] Number of monomers per star arm.
[c] From light scattering measurement in dilute cyclohexane (good solvent) solution [30, 32, 34, 51].

They are all nearly monodisperse with $M_w/M_n < 1.1$ (M_w being the weight average and M_n the number average molecular weights). The star polymers investigated in the context of this review are listed in table 1; note that some low functionality stars ($f = 4$) as well as the limiting case of a linear homopolymer ($f = 2$) are also included for comparison. It is interesting that the presence of an appreciable central core (for $f \geqslant 18$) creates a small but clear change in the glass transition temperature (as measured by differential scanning calorimetry) due to the restricted segmental mobility in that region. Functionality polydispersity (ε) is an important element here, and although very small, it proves very useful in exploring the dynamics of the stars, as discussed below. Based on the Daoud–Cotton analysis [36], multiarm star polymers constitute effective core–corona particles with core radius $r_c \sim f^{1/2}$ and softness [21] defined as $s = L/(L + r_c)$, L being the corona thickness; a typical value of s for the 128 arm stars is about 0.885.

Dilute star polymer solutions in a good solvent exhibit Brownian motion which can be detected using dynamic light scattering. From the measured scattering intensity $I(q)$, q being the scattering wavevector, the radius of gyration R_g can be determined (yielding the values given in table 1), whereas from the translational diffusion D_0, the hydrodynamic radius R_h can be extracted using the Stokes–Einstein relation [30, 31, 34, 35]. For a good solvent, the ratio R_h/R_g increases weakly with functionality, reaching values of 1.24 for $f = 18$, 1.28 for $f = 32$ and 1.4 for $f = 64$ or 128 [30, 32, 35, 51, 52]. One can appreciate the 'topological stretching' of the arms [36, 43, 48] by comparing the measured R_g values of 12 880 and PB165 (with molecular weight equal to the span molecular weight of the 12 880 star) in table 1, which conforms to the Daoud–Cotton scaling $R_g \sim f^{1/5} M_a^{3/5}$ [36].

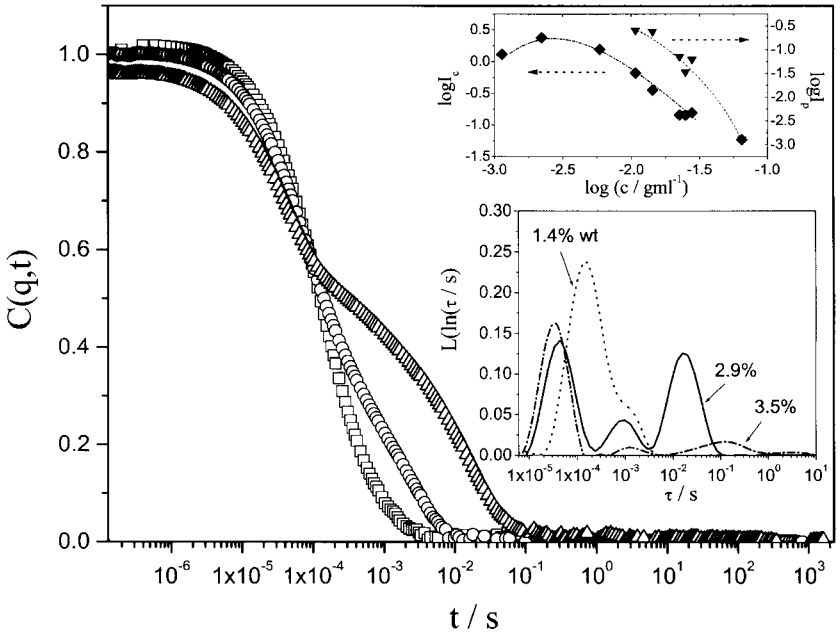

Figure 2. Normalized scattered field time autocorrelation functions $C(q, t)$ for 12 856 at three concentrations, namely dilute 1.4 wt% (□), and semidilute 1.8 (◯) and 2.9 wt% (Δ) in cyclohexane, and a value of the scattering wavevector $q = 0.035\ \mathrm{nm}^{-1}$. Upper inset: concentration dependence of the intensities of the cooperative I_c (♦) and slow self-diffusive I_p (▼) relaxation modes for 12 856/cyclohexane; the lines are drawn to guide the eye. Lower inset: the distribution of relaxation times $L(\ln(\tau))$ for different concentrations of 12 856 in cyclohexane, indicated in the figure; the appearance of the intermediate structural relaxation at higher concentrations is evident.

3. Relaxation dynamics in nondilute solutions

3.1. Collective dynamics

Above the overlap concentration in the interaction regime, the relaxation of concentration and density fluctuations takes place via three main mechanisms, namely, cooperative diffusion, self-diffusion and structural relaxation; whereas the first process is of polymeric nature, the other two relate to the colloidal character of the stars [32, 51]. A typical example is illustrated in figure 2, which depicts the normalized intermediate scattering functions $C(q, t)$ in the polarized geometry for three concentrations of 12 856 in the good solvent cyclohexane. $C(q, t)$ in the polarized geometry is given by $[(G(q, t) - 1)/f^*\,]^{1/2}$, where $G(q, t)$ is the light scattering intensity and f^* an instrument factor relating to the coherence area, obtained by means of a standard. In the dilute region $C(q, t)$ consists of a single exponential process, the translational diffusion [51, 52]; as the concentration increases above c^*, the presence of a second slower relaxation process is evident [51]. The separation of these two relaxations can be better appreciated with the inverse Laplace transformation (ILT) of $C(q, t)$ which is depicted in the lower inset of figure 2. It is further noted that both processes are diffusive (rate $\Gamma \propto q^2$) and characterized by q-independent intensities [51]. At the highest concentrations ILT reveals an intermediate relaxation process, as seen in the lower inset of figure 2, that is discussed later.

The faster process is identified with the cooperative diffusion of the entangled star arms, as it loses intensity (upper inset of figure 2) and becomes faster (short-time peaks in the lower inset

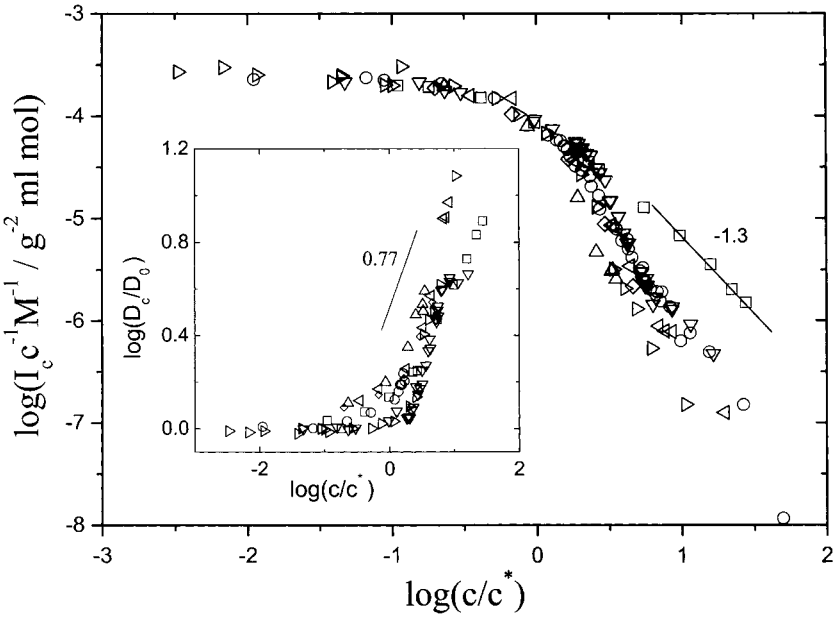

Figure 3. Intensity of the cooperative diffusion process (normalized with concentration c and total star molecular weight M) as function of the normalized concentration c/c^* (□, PBd165; ◯, 6407; △, 12 807; ▽, 12 814; ◇, 12 828; ◁, 12 856; ▷, 12 880). Inset: respective normalized cooperative diffusion (to the translational diffusion D_0) D_c/D_0 as function of c/c^*. Solid lines with slopes −1.3 and 0.77 represent the respective linear flexible chains scaling predictions.

of figure 2) as the concentration increases [8, 51, 53, 54]. Based on a single star polymer with self-similar structure of its blobs, the free energy F for semidilute solutions of stars with volume fraction ϕ was derived and consists of the classical ideal gas contribution ($\phi \ln \phi/(N_a f \upsilon)$ with υ the monomer volume) and an interaction term (excluded volume and stretching). The intensity of the cooperative process was subsequently calculated $I_c \propto (\partial^2 F/\partial\phi^2)^{-1}$ at the thermodynamic limit ($q = 0$) [51]:

$$\frac{I_c}{\phi M} \propto \phi^{\frac{-1}{3\nu-1}}\left[1 + 0.21(1+\delta)\left(\frac{\phi}{\phi^*}\right)^{\frac{-1}{3\nu-1}}\right] \tag{1}$$

where $M = N_a f$ is the molecular weight of the star, $\nu = 0.59$ is the Flory exponent, δ (>0) is the ratio of the elastic to the osmotic free-energy of the star colloidal core and $\phi^*\left(\sim\left(f^{1/2}/N_a\right)^{3\nu-1}\right)$ the crossover volume fraction when the outer blobs of the stars overlap. The above equation predicts the standard scaling behaviour of semidilute solutions of linear chains for $\phi \gg \phi^*$ and a steeper ϕ dependence in the region $\phi \cong O(\phi^*)$ as a result of the star architecture (whose contribution to the interaction free energy overwhelms the ideal gas free energy by $f^{3/2}$). This is confirmed experimentally [51, 53–56] as shown in the master plot of reduced I_c versus the reduced concentration, which is presented in figure 3. In contrast to the intensity behaviour, the cooperative diffusion of the semidilute hyperstar solutions is much less sensitive to f, although it does increase faster with concentration compared to the linear chain scaling [51]:

$$D_c = D_0\phi^{\nu/(3\nu-1)}\left[1 - 0.21\delta(\phi/\phi^*)^{-1/(3\nu-1)}\right] \tag{2}$$

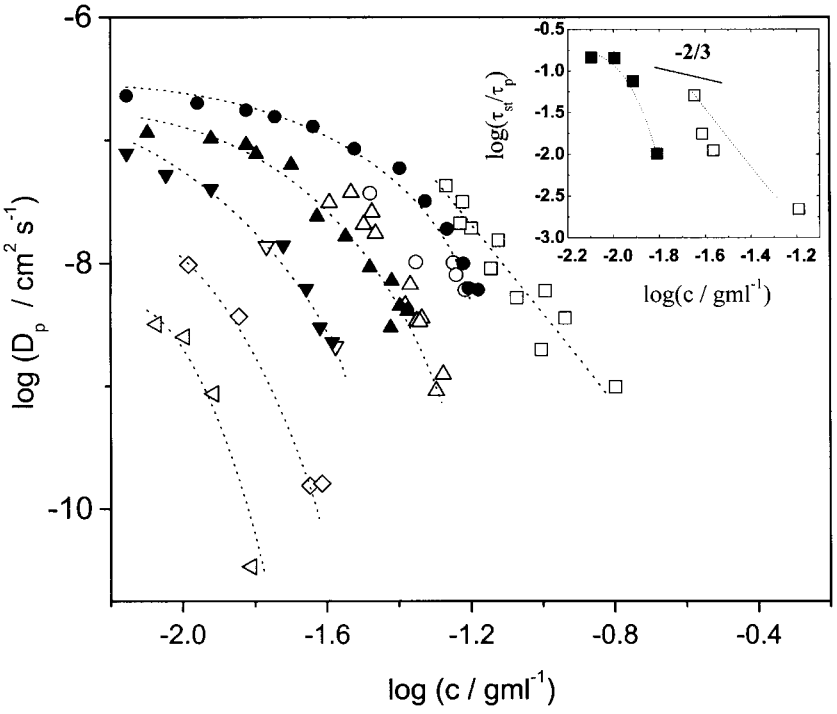

Figure 4. Concentration dependence of the diffusion coefficient D_p of the slow relaxation of thermal number density fluctuations (□, 6407; ◯, 12 807; △, 12 814; ▽, 12 828; ◇, 12 856; ◁, 12 880). Solid symbols represent respective PFG-NMR data confirming the assignment of this mode to the effective self-diffusion of the stars. Lines are drawn to guide the eye. Inset: concentration dependence of the ratio of the structural to the slow (polydispersity) relaxation times, τ_{st}/τ_p, for 12 856 (■) and 12 880 (□), taken at $q = 0.035\ \mathrm{nm}^{-1}$. Lines are drawn to guide the eye. The line with slope $-2/3$ represents the scaling prediction (see text).

where D_0 is the single star translational diffusion. This behaviour is experimentally confirmed with the multiarm stars of $f = 64$ and 128, as demonstrated in the inset of figure 3.

The slow diffusive process represents the relaxation of thermal number density fluctuations and is associated with the star self-diffusion. In analogy to size polydispersity effects in colloids [57], finite functionality polydispersity (ε) of the stars (see table 1) can cause density fluctuations due to the exchange of two effective populations, namely small $f(1-\varepsilon)$ and large $f(1+\varepsilon)$ stars. In the limit of small polydispersity $\varepsilon \ll 1$, there is no phase separation and the process is driven by the ideal gas entropy of mixing of the two types of stars and hence the intensity and decay rate of the slow process are [32, 51]

$$I_p \sim \frac{f^2\varepsilon^2}{N_a}\phi^{\frac{3\nu-3}{3\nu-1}} \propto \phi^{-1.6} \qquad \text{and} \qquad \Gamma_p \cong D_p q^2. \tag{3}$$

This assignment is based on the grounds of an excellent agreement of the slow diffusion coefficients, D_p, with independent measurements of star self-diffusion using pulsed field gradient NMR (PFG-NMR) [32, 51], as demonstrated in figure 4.

The upper inset of figure 2 depicts the concentration dependence of the intensity of the slow mode I_p, which appears to conform to the prediction of equation (3) [51]. The fact that I_p drops as the concentration of stars increases is suggestive of their interpenetration (also demonstrated by the cooperative intensity drop, shown in the same plot), which results in a

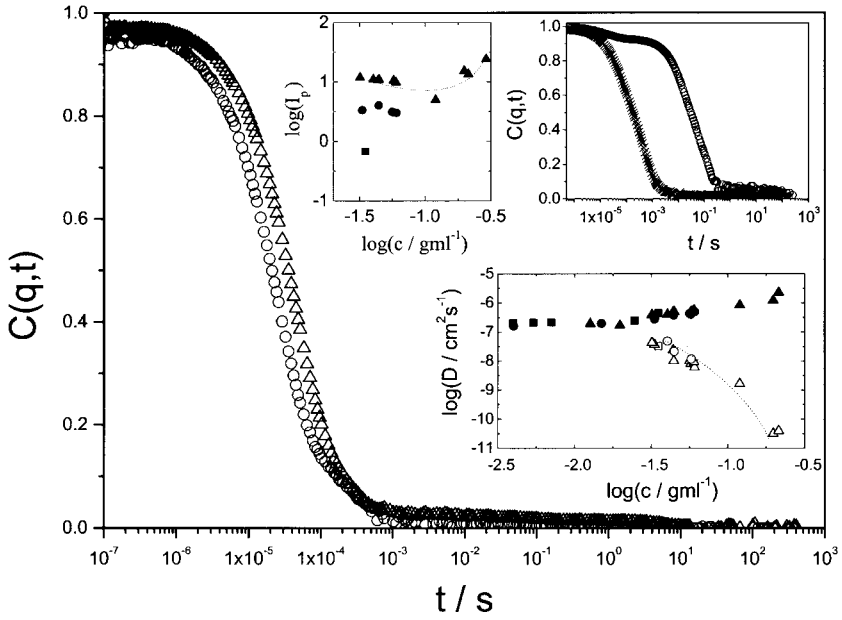

Figure 5. Intermediate scattering functions $C(q, t)$ for 12 807 (◯) and 3210 (△) 4.5 wt % in cyclohexane and $q = 0.033$ nm^{-1}. Upper left inset: concentration dependence of the intensity of the slow self-diffusive relaxation mode (■, 3210; ●, 12 807; ▲, equimolar blend solution 12 807/3210 in cyclohexane). The line is drawn to guide the eye. Upper right inset: $C(q, t)$ for an equimolar 12 807/3210 blend solution in cyclohexane with total polymer concentration 4.1 wt% (×) and 15.4 wt% (◯), at $q = 0.025$ nm^{-1}. Lower inset: concentration dependence of the cooperative diffusion (solid symbols) and slow self-diffusion coefficients (□, 3210; ◯, 12 807; △, equimolar blend 12 807/3210). Line is drawn to guide the eye.

reduction of the effective refractive index contrast between the core region and the semidilute arm solution. An interesting implication from equation (3) is that the quantity I_p/f^2 should be independent of f; this was indeed confirmed using data from the stars listed in table 1 [58]. Given its assignment, the diffusion coefficient D_p of this slow process should scale with the inverse solution (zero shear) viscosity over a wide concentration range. This is indeed demonstrated in the inset of figure 6.

In addition to the above considerations, mixing of stars of different functionalities enhances the apparent functionality polydispersity rendering the detection of the self-diffusive mode with light scattering clearer even at lower concentration. This effect is demonstrated in figure 5 which depicts the normalized intermediate scattering function $C(q, t)$ for two stars of different functionality and nearly the same arm molecular weight, namely 12 807 and 3210, each at 4.5 wt% in cyclohexane, along with their equimolar 50/50 mixture (total concentration 4.1 and 15.4 wt% in cyclohexane; upper right inset of figure 5), having an average effective functionality $\langle f \rangle = 80$ [58]. The higher intensity I_p of 12 807 compared to 3210, as seen in the upper left inset of figure 5, can be rationalized on the grounds of equation (3) because of different f, reflecting the different topology [58]. A remarkable slowing down over nearly four decades is observed in the self-diffusion for a concentration increase of about one decade, as shown in the lower inset of figure 5. In particular, at the two highest concentrations measured D_p falls by nearly two decades, while the sample remains ergodic at all times. At the same time the self-diffusion coefficients of both the mixture and each of the components are identical (lower inset figure 5), suggesting a competition between the large size of more dense

stars (12 807) and the enhanced viscous drag in the looser fractal structures of low-f stars (3210), in controlling the self-diffusive motion. Therefore, as the concentration increases, the separation between polymeric and colloidal contributions to the dynamics of multiarm star polymers is enhanced; the cooperative process becomes faster and loses intensity in favour of the self-diffusion mechanism, which becomes stronger and controls the relaxation process with a dramatic slowing down.

At the highest concentrations for the largest stars a third intermediate relaxation process can be observed, as clearly evidenced from the ILT of the $C(q, t)$ of 12 856 2.9 and 3.5 wt% in the lower inset of figure 2. It is attributed to the spatial correlations between the star centres due to the liquid-like ordering, which relax via collective structural rearrangements, in analogy to suspensions of colloidal hard spheres and micelles [22, 51, 59, 60]. The reason that this relaxation mode was detected only for the largest stars available (12 856 and 12 880) is because only for these systems $qR \sim O(1)$. From the limited data obtained, it can be observed that the intensity and the (non-diffusive) relaxation time increase with q [32, 51]. As the structural process involves essentially local rearrangements of the stars, its relaxation time is of the order of the star self-diffusion over a distance of its size, R_0, $\tau_{\rm st} \sim R_0^2/D_p$. Using equation (3) for the slow time $\tau_p = \Gamma_p^{-1}$, we arrive at $\tau_{\rm st}/\tau_p \sim q^2(Nf\upsilon/\phi)^{2/3} \propto \phi^{2/3}$ [51]. The limited data for 12 856 and 12 880 in the inset of figure 4 suggest that this simple theoretical argument does not hold in the range of high concentrations well above c^*. It is clear however, that a more rigorous analysis of this process requires larger stars in order to reach the regime $qR > 1$. As such stars were not available, this task was accomplished with the use of very high molecular weight diblock copolymer micelles, which exhibit several common features with the stars [22]. In addition, in these systems, shape fluctuations of the star-like structures (breathing modes), predicted by simulations [61] could be evidenced; however, given the fact that these two systems exhibit differences as well [22, 58 and relevant discussion], this will not be discussed further in this review.

3.2. Viscosity and self-diffusion

Figure 6 depicts the concentration dependence of the viscosity. It actually plots the zero shear viscosity (measured in steady shear flow by capillary viscosimetry [62] or conventional rheometry [63]) against the effective hydrodynamic volume fraction $\phi_{\rm eff}$, which is actually c/c^*, the c^* being estimated from the *hydrodynamic* radius R_h [63]. In this plot hard sphere data are included as well, taken from the literature [59]. They serve as a guide for appreciating the molecularly tunable softness of the multiarm star polymers, which can essentially range from soft colloidal spheres ($f = 128$ with small departure from hard sphere behaviour) to entangled polymers ($f = 32$). Fitting of these data with semi-empirical expressions for the concentration-dependent viscosity, such as the Krieger–Dougherty equation, yields maximum packing volume fractions $\phi_m > 0.59$, the hard sphere limit. This is typical for sterically stabilized soft colloids [64–66], and here it is a consequence of the star interpenetration. The softness of the different stars relates to the star–star interaction that was recently quantified by Likos *et al* [33], who proposed an interaction potential with a Yukawa soft form at long distances and a strong logarithmic repulsion at short distances.

Additional information on star dynamics and their interplay with structure is obtained from the PFG-NMR experiment, which essentially measures directly the incoherent structure factor of the star $S_{\rm inc}(q, t)$. In the Gaussian approximation we can write [67]

$$S_{\rm inc}(q, t) = A \exp(-q^2\langle\Delta r^2(t)\rangle/6) \tag{4}$$

where $\langle\Delta r^2(t)\rangle$ is the mean-square displacement. For free diffusion, $D_s = \langle\Delta r^2(t)\rangle/6t$ (based on the above discussion we consider that the self-diffusion coefficient $D_s = D_p$) and hence

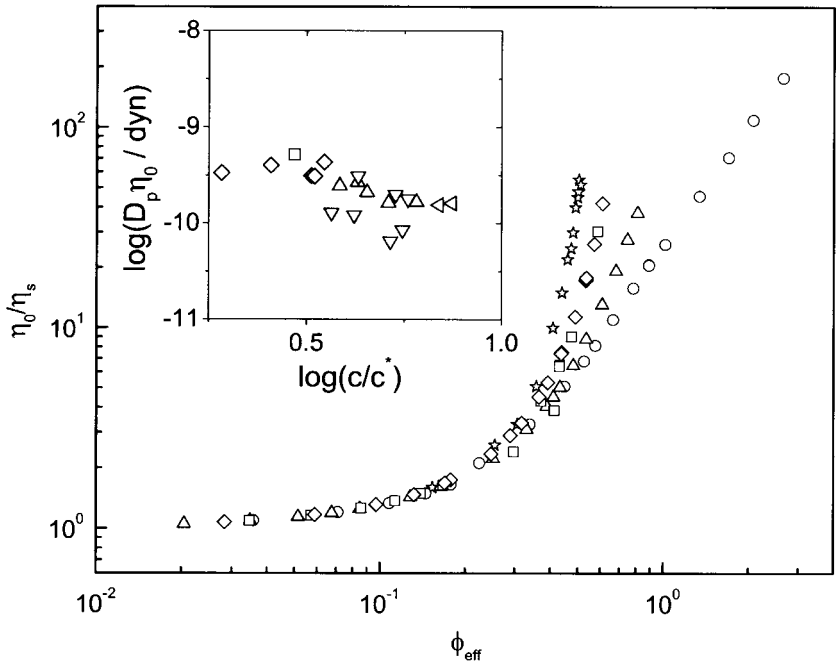

Figure 6. Relative zero-shear viscosity (normalized to the solvent η_s) η_0/η_s as a function of the effective volume fraction ϕ_{eff} (the equivalent of c/c^* in stars using their hydrodynamic radius) for different stars: 3280 (◯), 6407 (△), 12 807 (◇) and 12 880 (□); the hard sphere limit is represented by data on 640 nm PMMA particles in decalin (☆) [59]. Inset: concentration (c/c^*) dependence of the product of slow (self) diffusion coefficient to zero shear viscosity $D_p\eta_0$ for different multiarm star polymers (△, 6407; ◇, 12 807; ▽, 12 814; □, 12 828; ◁, 12 856).

$S_{\text{inc}}(q, t) \sim q^2 t$, as shown in figure 7 for a 5 wt% solution of 12 807 in D-toluene . At the highest examined concentration (7.3 wt%) $S_{\text{inc}}(q, t)$ was found to exhibit a non-diffusive behaviour (upper inset of figure 7 with probing times between 33 and 303 ms); it revealed only in-cage diffusion with time-independent amplitude (equation (4)) $\langle \Delta r^2(t) \rangle^{1/2} \approx 70$ nm, indicative of a spatial localization of the stars (lower inset of figure 7). Free in-cage diffusion would require probing times faster than 33 ms (and short qs), whereas observation of a long-time diffusion may be possible for $t > 303$ ms. It is noted that for concentrations between 5 and 7.3 wt%, the purely diffusive fraction of $S_{\text{inc}}(q, t)$ decreases with c, and for $c = 7.04$ wt% both a long-time free diffusion and in-cage localization with $\langle \Delta r^2(t) \rangle^{1/2} \approx 300$ nm was observed for times longer and shorter than 70 ms, respectively [68]. Furthermore, the transition from free diffusion to in-cage diffusion occurs at about 7 wt% where the formation of macroscopic gelation is observed and dynamic light scattering reveals slow cluster-like processes and some non-ergodicity [55, 69]. This is in constrast to reports on the presence of such processes in stars of much lower functionality ($f = 18$) [70]. It is also worth mentioning that preparation of molecularly dispersed solutions is a non-trivial task involving persistent gentle stirring at very low concentrations. The full picture can be visualized by computer simulations of the centre-of-mass mean-square displacements of the stars, depicted in figure 8(a) for a dense star system with $f = 48$ and $N_a = 20$ [40]. A similar crowding effect can be observed in solvents of intermediate quality, like decane in the present case, as a function of temperature at constant mass concentration. In such situations, the single star swells upon heating and in the

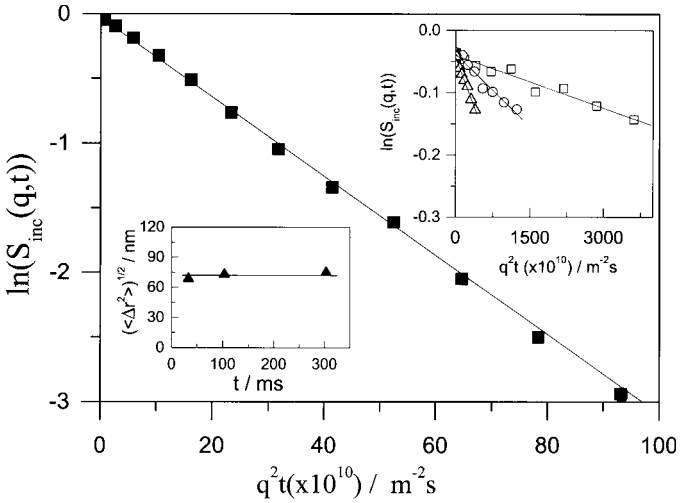

Figure 7. Representation of the incoherent structure factor $S_{\mathrm{inc}}(q, t)$, obtained from PFG-NMR, versus q^2t for a 5 wt% D-toluene solution of 12 807 (■), exhibiting a single diffusive process (the solid line is the least square fit to the data). Upper inset: respective plot for higher concentration (7.3 wt%), exhibiting non-diffusive character (probing times: Δ, 33 ms; ◯, 103 ms; □, 303 ms) and revealing in-cage diffusion. Lower inset: representation of spatial localization of the stars from the upper inset, yielding a mean-square displacement of about 70 nm.

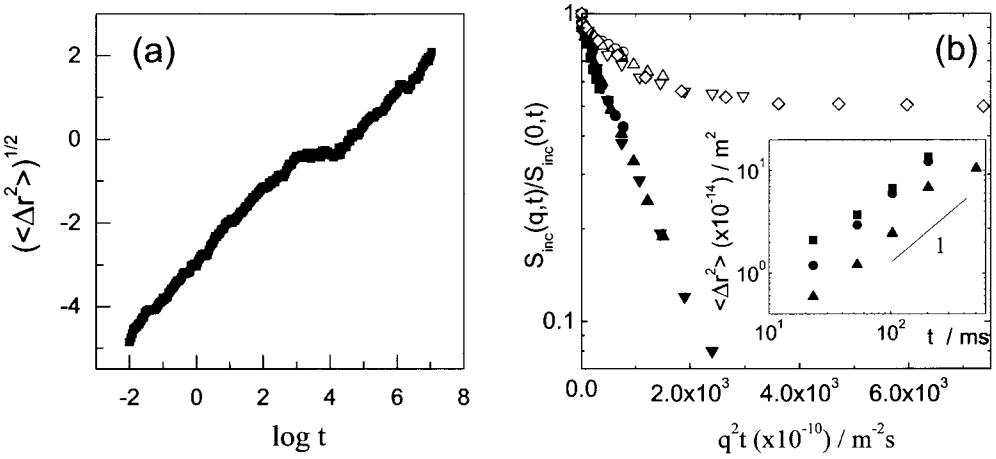

Figure 8. (a) Monte Carlo computer simulations of mean displacement amplitude $\langle \Delta r^2 \rangle^{1/2}$ versus time for a dense star system with $f = 48$ and $N_a = 20$, exhibiting an early free diffusion, a subsequent in-cage diffusion, and a long-time free diffusion. (b) Normalized incoherent structure factor $S_{\mathrm{inc}}(q, t)$ as function of q^2t for 12 828/D-decane 8.3 wt% at different measurement times (▷, 23 ms; ◯, 53 ms; Δ, 103 ms; ▽, 203 ms; ◇, 503 ms). Solid symbols denote low temperature (25° C) and open symbols high temperature (50° C). The former indicate Fickean diffusion (also plotted in the inset as mean square displacement against time), whereas the latter show the frozen motion at high temperatures.

semidilute and concentrated regions the swelling causes an increase of the effective volume fraction. Figure 8(b) shows that the $S_{\mathrm{inc}}(q, t)$ of 12 828 8.3 wt% in D-decane at low temperature (25 °C) is representative of free Fickian diffusion (inset). In contrast, at higher temperature

(50 °C) the freezing of the self-diffusion at long times relates probably to the presence of clusters rather than the cage effect (since the q^2t scaling still holds) [71].

4. Viscoelastic response in the melt

The dynamic response of the multiarm stars in the melt was studied with small amplitude oscillatory shear measurements under a nitrogen atmosphere over a wide range of temperatures (from −103 to 150 °C) [50, 72]. A typical result of the measured dynamic storage and loss moduli, G' and G'' respectively, is depicted in figure 9 for the samples 12 828 (a) and 6430 (b). Due to the wide frequency range obtained from time–temperature superposition, the various regimes of viscoelastic relaxation can be clearly detected. Starting from the higher frequencies, we note the glass transition region (extending up to the crossover frequency ω_s), the Rouse-like transition regime (ω_e), the rubber plateau (ω_R) and the terminal region. Of particular interest is the latter, since it is characterized by a two-step decay, in sharp contrast to the single terminal relaxation processes of the low functionality stars, linear homopolymers or colloidal hard spheres. The corresponding relaxation modulus $G(t)$ for 12 828, obtained from the Fourier transformation of the $G'(\omega)$ and $G''(\omega)$ data, is shown in the inset of figure 9(a) as a function of time. Such a representation helps identify the two terminal processes, typically by fitting the long time region beyond the plateau G_N^0 with a sum of two stretched exponentials, which can eventually yield information on the distribution of relaxation times [73]. All polybutadiene stars and their linear counterparts studied were found to have the same G_N^0, implying that they have the same entanglement molecular weight, M_e. In addition, they all exhibited the same thermorheologically simple behaviour, as indicated in the inset of figure 9(b), which depicts the temperature dependence of the frequency shift factor α_T. The well-known WLF expression $\log \alpha_T = -c_1(T - T_{\rm ref})/(c_2 + T - T_{\rm ref})$ [74] represented all data well with $T_{\rm ref} = 190$ K and fitted values $c_1 \approx 12$ and $c_2 \approx 50$ K.

The faster of the two relaxations in the terminal region (ω_R) is due to the star arm relaxation, as demonstrated by its independence of functionality (vertical dotted arrows in figure 9) [50, 72, 75–77]. Recently, Milner and McLeish presented a parameter-free theory for the arm relaxation, using the concept of dynamic dilution with the appropriate scaling of entanglement length, and incorporating the effects of higher Rouse modes on arm retraction [78, 79]. This theory was developed in the framework of the tube model and was proven successful in describing the arm relaxation of low functionality stars of different chemistry [78, 80]. It captures quantitatively the arm relaxation of multiarm stars as well, as demonstrated in figure 9 (solid lines) and discussed in detail elsewhere [81]. There are no adjustable parameters in this theory as the only ones used, namely the entanglement molecular weight M_e, respective plateau modulus G_N^0 and the (Rouse) relaxation time of an entanglement segment τ_e, are determined from the data. This confirms the assignment of the faster terminal mode to arm relaxation (fluctuations). The complex viscoelastic modulus $G^*(\omega)$ is obtained from

$$G^*(\omega) = (x+1)G_N^0 \int_0^1 {\rm d}s\,(1-s)^x \left[\frac{{\rm i}\omega\tau(s)}{1+{\rm i}\omega\tau(s)}\right]$$

where s is the relaxed fraction of the arm. The total arm relaxation time is a function of the potential $U_{\rm eff}$,

$$\tau(s) = \left(\frac{{\rm e}^{-U_{\rm eff}(s)}}{\tau_{\rm early}(s)} + \frac{1}{\tau_{\rm activated}(s)}\right)^{-1}$$

incorporates an early fast diffusion of the free end of the arm and an activated arm retraction, and depends on τ_e and the number of entanglements per arm. The latter is reduced by the

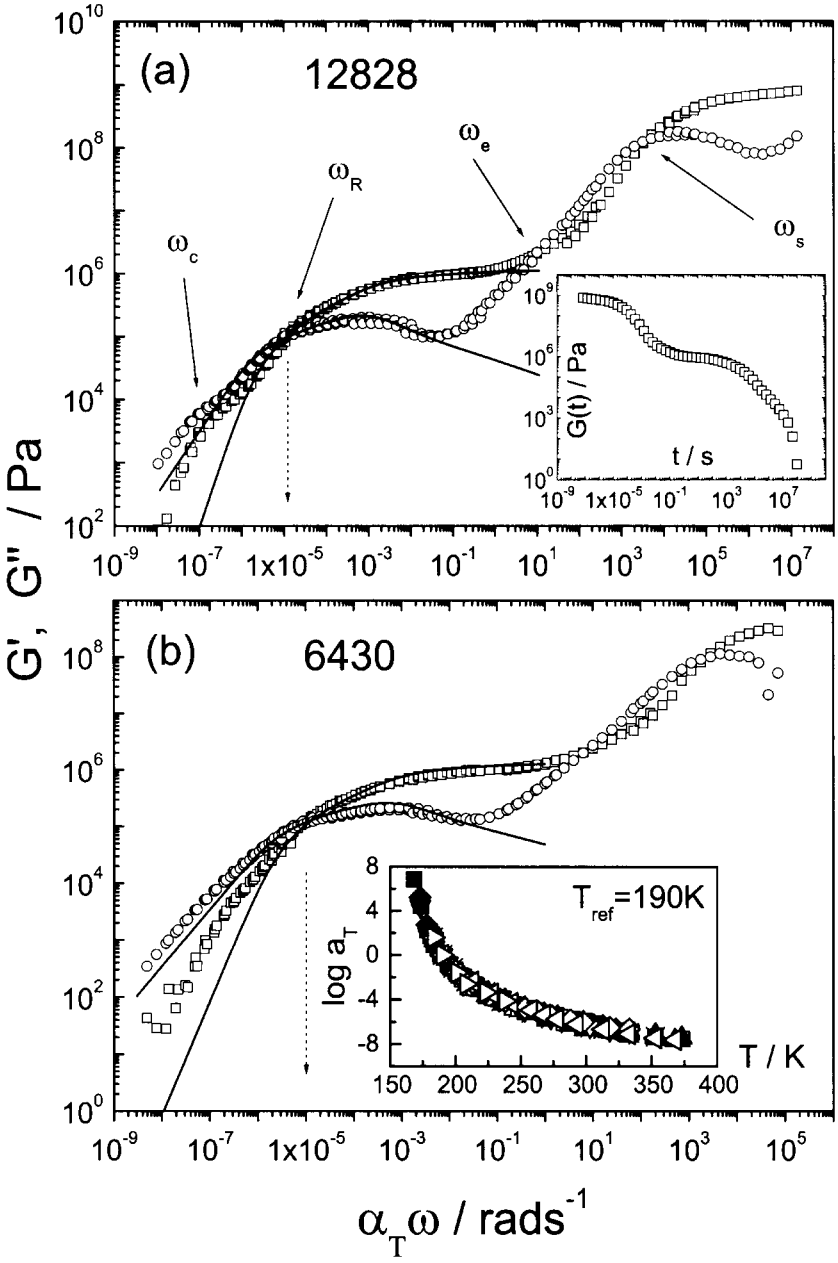

Figure 9. Master curves of elastic storage (G', □) and viscous loss (G'', ○) linear viscoelastic moduli of the 12 828 (a) and 6430 (b) star polymers in the temperature range from 150 up to −103 °C, with reference temperature −83 °C. Solid arrows represent the various transitions and corresponding crossover frequencies (ω_s: glass to Rouse-like transition; ω_e: transition to rubber plateau; ω_R: terminal–arm relaxation; ω_c: terminal–structural relaxation). Vertical dotted arrows indicate the (inverse) arm relaxation times, which are independent of functionality. The solid lines represent the predictions of the Milner–McLeish theory [78] for the arm relaxation process (see text), for G' and G''. Inset to (a): linear relaxation modulus $G(t)$ as function of time for 12 828. Inset to (b): frequency shift factor α_T against temperature for a variety of stars and linear chains (⊞, PB165; ⊕, 4S40; ×, 4S120; ■, 6407; ●, 6415; ▲, 6460; ▼, 12 807; ♦, 12 814; □, 1518; ○, 2518; △, 3718; ▽, 3216; ◇, 3220; ◁, 3237; ▷, 3280).

dynamic dilution effect as $M_e(s) = M_e/(1-s)^x$, with $x = 4/3$ [82, 78, 79]. The analysis of the multiarm star data using this theory considers that a small fraction of the arm near the centre is included in the core and does not contribute to this process [81].

Further support to the assignment of the various relaxation processes in the star melts comes from Monte Carlo computer simulations using the cooperative motion algorithm [40, 50, 72, 83]. In general, complex polymeric systems, such as melts of multiarm stars or melts of micelles in microphase-separated block copolymers exhibit a complex dynamic behaviour resulting from the ordering of macromolecules or micelles. Results of simulated dense systems of this kind of macromolecule have shown that the structure develops due to a strong excluded volume effect between structural elements on the macromolecular scale. This leads to additional dynamic relaxation modes, which although taking place on the macromolecular size scale, have many similarities with the cooperative rearrangements considered in the dynamic lattice liquid model [84] for the dynamics of small molecules in a simple liquid. In this type of simulation, the pair correlation functions of star centres of mass clearly indicate an enhanced ordering with increasing number of arms, which strongly resembles the cage effect of liquids. However, in the case of multiarm stars this effect relates to the macromolecular size scale. The formation of this structure involves considerable changes in the dynamics of multiarm star melts with respect to melts composed of stars with a low number of arms. The flow of such systems is controlled not by the star arm relaxation but by an additional slow relaxation process which has been attributed to cooperative rearrangements of stars within the ordered state [40, 84, 72, 76]. As demonstrated in figure 10(a), the latter process involves the slowing down of the decay of the position correlations of such stars $\rho_c(t)$, which for a large number of arms become considerably slower than the relaxation of star arms $\rho_R(t)$ (figure 10(b)), and of course the segmental relaxation $\rho_s(t)$ (figure 10(b)), constituting in this way an extra slow mode in the translational relaxation [76, 84].

Figure 11 represents the dependence of the arm relaxation time under isofrictional conditions (normalized to the segmental time) τ_a/τ_s on the arm degree of polymerization, N_a, for a variety of star polymers with functionality ranging from 4 to 128 and two different chemistries, 1, 4-polyisoprenes and 1, 4-polybutadienes. The linear data are included in order to appreciate the important effect of branching in enhancing the arm relaxation time for the same molecular weight (with the star arm) above M_e [75, 79]. The interesting feature of this plot is its generic validity for all these different systems (also in good agreement with simulation results [40, 72]), suggesting a universality of the arm relaxation behaviour. In addition, in the regime of low molecular weights below the entanglement threshold, the arm relaxation follows Rouse-like behaviour. This was demonstrated with data from star-like polymacromonomers of styrene and poly(methyl methacrylate) [85] and confirmed by computer simulations as well [40, 72]. A linear unentangled polystyrene is also included in figure 11 along with the polymacromonomers, and does not show much difference as expected in this molecular weight regime. Further, the arm relaxation τ_a/τ_s can also be plotted against the number of entanglements per arm N_a/N_e yielding a generic behaviour for all entangled stars (figure 11(b)), as expected from the Milner–McLeish theory and seen before for low-f stars only [75, 86, 87].

The slow relaxation process (ω_c) in figure 9 relates to the topological heterogeneity of the multiarm stars, which leads to a liquid-like ordering even in the melt, as seen in the SAXS profiles in figure 12. It is apparent that for the three stars investigated, in addition to the first sharp and intense peak, there are broader and less intense higher order peaks, approximately at positions $\sqrt{3}$ and $\sqrt{7}$ with respect to the first one [72], indicative of an ordered liquid state. The distances between neighbouring star centres were determined from $d = a/s_{\text{peak}}$ with $s_{\text{peak}} = q_{\text{peak}}/2\pi$ and $a \approx 1.23$ for a structure controlled only by two-body correlations.

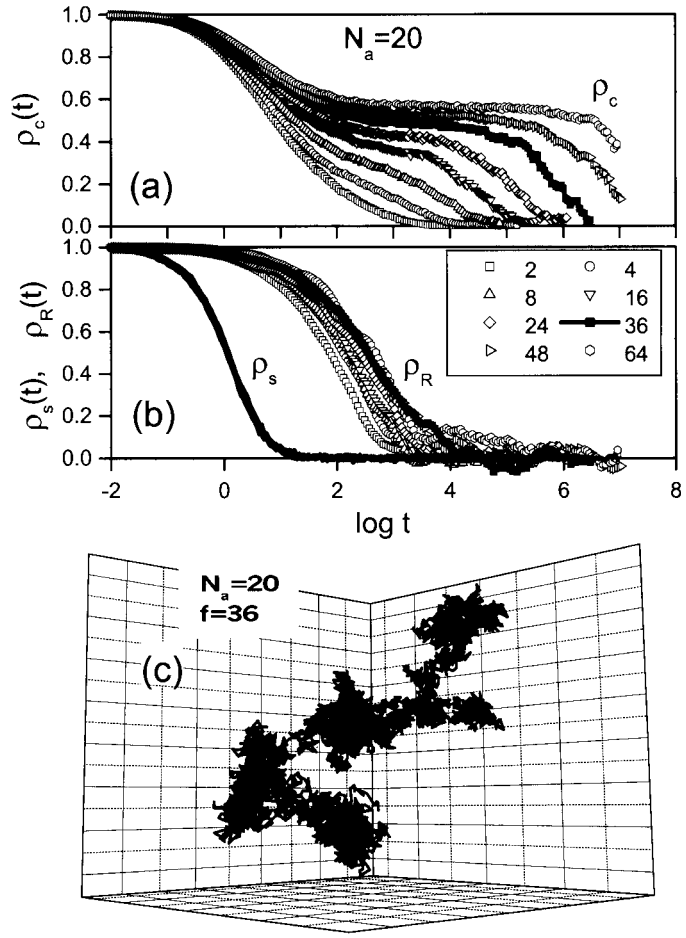

Figure 10. Time autocorrelation functions for simulated melts of stars with $N_a = 20$ and varying arm functionality (including the linear chain limit $f = 2$). (a) Positions of star elements $\rho_c(t)$ representing the motion of the whole stars ; (b) segment positions $\rho_s(t)$ representing local dynamics and centre-to-end vectors of arms $\rho_R(t)$ representing star arm relaxation; (c) a typical star centre-of-mass trajectory recorded for a multiarm star with $f = 36$. The trajectory consists of blobs related to a longer residence of the star at some well-distinguished places which are regularly distributed along the trajectory and are connected by thinner trajectory fragments related to faster displacements between the localized states.

In the present dense star melts, these values are considered as approximate star sizes which satisfy the relation $d \sim M_a^{1/3}$, as seen in the inset of figure 12. The experimental as well as the simulation results show that the degree of order in star polymer melts depends on both molecular parameters, i.e. the number and the length of the arms. Actually, it can be concluded that the degree of order in the studied systems is mainly controlled by the ratio of the core radius to the corona thickness. Therefore, for stars with a large number of short arms the highest degree of ordering should be expected, whereas stars with long arms could show a limited order even when the number of arms is high. The type of order observed in the multiarm star melts (as well as in the nondilute solutions) can be described as liquid like on the macromolecular scale. Neither in real nor in simulated systems, have any clear signatures of lattice formation been detected [40, 50, 72]. This results probably from the substantial

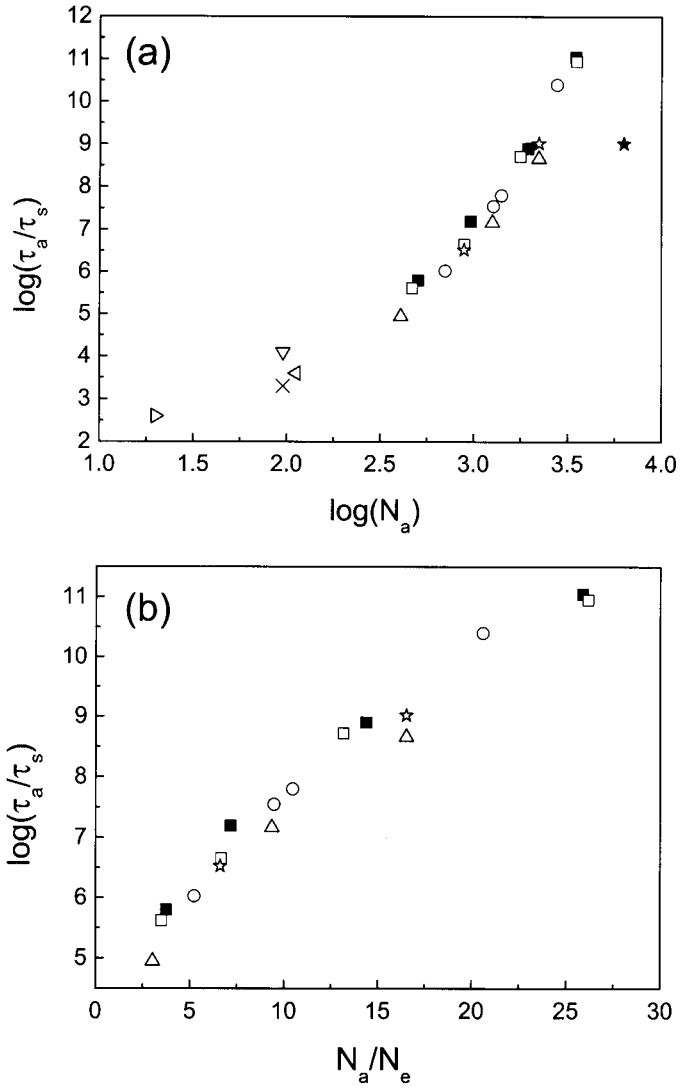

Figure 11. Normalized arm relaxation time (to the segmental time τ_s) τ_a/τ_s against arm degree of polymerization N_a (a) and number of entanglements N_a/N_e (b), for various star functionalities studied (☆, $f = 4$; Δ, $f = 18$; ○, $f = 32$; □, $f = 64$; ■, $f = 128$). The linear chain PB165 data point (★) is also included for comparison. To complete the picture, some data are also included from low molecular weight (below M_e) star-like polymacromonomers with polystyrene arms with functionality $f = 10$ (◁, $M_a = 10000$ g mol^{-1}; Δ, $M_a = 11800$ g mol; ▷, $M_a = 2100$ g mol^{-1}) [85], along with a linear polystyrene chain with $M_a = 10000$ g mol^{-1} (×).

deformability and related form fluctuations of the star coronas [35, 61]. They consist of flexible arms and remain soft spheres even when the number of arms and the core radius are large. The latter is well confirmed by the dynamic properties of the studied systems. Similar behaviour has been observed in various other systems, such as microgels [76] or polymer melts filled with spherical copolymer micelles [17, 18]. In all these cases, the ordering was related to the excluded volume interaction between compact but deformable macromolecular elements in a dense system [50, 76]. These findings, however, contrast the predictions for stars [49, 88, 89]

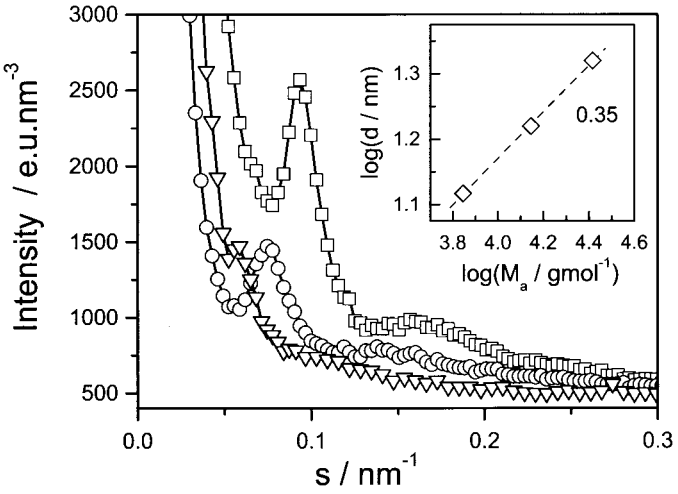

Figure 12. SAXS intensity distributions of star melts 12 807 (□), 12 814 (○) and 12 828 (∇), at 20 °C; $s = q/2\pi$ with q the scattering wavevector. Inset: corresponding dependence of the estimated distances between neighboring centres (approximately star sizes) $d \approx 1.23/s_{\text{peak}}$ [72] as a function of the arm molecular weight, M_a.

as well as experimental findings in block copolymer micelles [14, 15, 90, 91], indicating some kind of macrocrystalline ordering. A possible suggestion for weak crystal formation at high concentrations is implied from PFG-NMR data showing a dramatic slowing down of the self-diffusion coefficient [68], but a direct experimental confirmation is still lacking.

Therefore, the suggested assignments of the relaxations detected by means of the viscoelastic measurements appear to be reflected in the simulations. As already discussed in the context of figure 10, two relaxations, one related to segmental motion $\rho_s(t)$ and the other to star arm relaxation $\rho_R(t)$, are observed in all systems (figure 10(b)). The relaxation rate of the first one is independent of star structural parameters both in experiments and in the simulation. On the other hand, the star arm relaxation is observed to be considerably dependent on the arm length but virtually independent of the arm number. The most interesting effect observed both in the simulated (hyperstars with rather low N_a compared to the experimental systems) and in the real systems is the additional slow relaxation process appearing in systems with clear ordering of stars, and unambiguously observed for $f > 32$ (note that for linear chains and low-f stars $\rho_R(t)$ and $\rho_c(t)$ are virtually identical). The analysis of the simulation results concerning the slow dynamics (figure 10(a)) is further supported by the direct observation of star motions in these systems (figure 10(c)). The shown simulated trajectory of a star centre in the melt is nonuniform in time. It comprises fragments whose motion consists of limited excursions from some quasi-localized positions (black blobs in figure 10(c), which are connected to other fragments indicating occasional fast displacements between 'localized' states, and suggesting analogies to the self-diffusion measurements of figure 8. The amplitude of excursion and time of residence in such a 'localized' state depend strongly on the star arm number and length. These results suggest that the slow process can be attributed to translational cooperative rearrangements of stars (on macromolecular scale) within the ordered state which are of the same character as those suggested for the cooperative rearrangements in low molecular liquids [92].

Naturally, because of the presence of the slow relaxation, the zero shear viscosity η_0 is no longer independent of the functionality f (but only the arm relaxation time τ_a), as in the case of low-f stars [50, 75, 79, 93]. A slow viscoelastic relaxation was also observed for the case

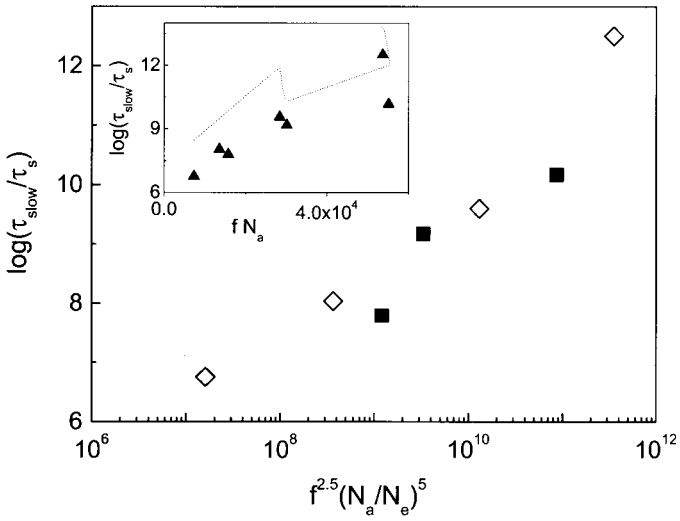

Figure 13. Normalized slow relaxation time (to the segmental time) $\tau_{\rm slow}/\tau_s$ against $f^{2.5}(N_a/N_e)^5$ for multiarm stars with functionality $f = 64$ (◇) and $f = 128$ (■), for which a slow process was detected. Inset: dependence of $\tau_{\rm slow}/\tau_s$ on fN_a. The apparent scattering in the data (▲) relates to the different combination of f (64 or 128) and N_a. The dotted lines represent the theoretical prediction (equation (5)).

of block copolymer micelles in selective solvents, and attributed to the translational motion of the ordered objects [15, 94].

A mean-field scaling theory of the slow mode suggests that this structural mode, which takes place cooperatively, is an activated process and involves a partial disentanglement of the interpenetrating stars followed by a displacement of the star in a neighbouring cell, a distance of its size apart, a process controlled by the free energy of the corona elastic deformation (arm stretching). The net result of this analysis suggests the following scaling relation [81]:

$$\frac{\tau_{\rm slow}}{\tau_s} \sim \alpha^{-1/3} f^{11/9} N_a^{26/9} N_e^{-1} \exp\left[\frac{X_1}{\alpha}\frac{f^{5/3}}{N_a^{1/3}} + X_2\alpha^2\frac{N_a^{11/3}}{N_e^3 f^{4/3}}\right] \tag{5}$$

where $\alpha = a^2\upsilon^{-2/3}$, a is the monomer size, and X_1 and X_2 are unspecified numerical constants. The main outcome is the strong dependence of the structural relaxation on both functionality and arm molecular weight, in qualitative agreement with the experimental findings from the stars for which the slow process could be detected ($f = 64$ and 128). For these systems, the extracted slow times were found to scale approximately with arm functionality and molecular weight as $\tau_{\rm slow}/\tau_s \sim f^{2.5}N_a^5$. Actually, figure 13 depicts $\tau_{\rm slow}/\tau_s$ against $f^{2.5}(N_a/N_e)^5$. Given the uncertainty of this scaling (only two functionalities, 64 and 128), it is apparent that the behaviour of the stars is rather universal with respect to their structural relaxation as well. Moreover, the qualitative agreement of the theoretical prediction (equation (5)), as reflected in the inset of figure 13 (predictions are indicated by the dotted line using typical values for the numerical constants $X_1 = 0.0040$ and $X_2 = 0.0075$), is evident.

5. Conclusions and outlook

The dynamic response of multiarm star polymers reflects their hybrid polymer–colloid character. The star arms are responsible for the former and the whole macromolecular

objects for the latter. In the solution above c^*, concentration and density fluctuations relax via polymeric cooperative diffusion and colloidal self-diffusion and structural relaxation. The dependence of the collective and self-dynamics on concentration reflects the star topology (stretched arms) and distinguishes the star behaviour from that of linear flexible homopolymers. In the melt state, the two-step viscoelastic relaxation in the terminal region signifies the faster polymeric arm relaxation and the slower colloidal structural rearrangements of the weakly ordered stars, a consequence of macromolecular excluded volume. Computer simulations and analytical theory assist in the assignment of the relaxation modes and the identification of the star's unique and universal features.

These novel soft materials represent model systems that combine both polymeric and colloidal characteristics, and thus bridge the gap between polymer science and colloid science. Our understanding of their properties will eventually allow us to design materials and supramolecular assemblies with desirable intermediate properties. Within this general framework and with the current level of understanding of the dynamics of model multiarm star polymers, progress can be made in the exploration of the dynamic properties of more complex 'hybrid' polymeric–colloidal materials sharing inherent density inhomogeneities and exhibiting common features with the hyperstars. They include, but are not limited to, 'irregular' multiarm stars with very high functionality (270 arms) and nonspherical central core [95, 96], bottlebrush structures formed from polymacromonomers [97, 98], self-organized superstructures resulting from telechelic linear and star homopolymers and copolymers [99–103], hyperbranched polymers with varying number of generations and controlled molecular weight [104, 105], supramolecular polymers [106], dendrimers [107], functionalized dendritic structures [108], polyelectrolyte brushes [109, 110], copolymer-based microemulsions [111], tethered chain systems [112], micelles with chemically fixed core [113], microgel-based self-assemblies [114], comb-like macromolecules [115], star–star and star–linear chain mixtures [116–121], mixtures involving soft spheres, hard spheres and linear chains [122–124] and hairy-rod polymers [125–127]. An important asset in such an ambitious research program is the predictive ability stemming from computer simulations [40, 83, 84, 92] as well as rigorous theory. Concerning the latter, recent successes include the analysis of the rheology of Cayley tree structures [128], the pom-pom model [129], and the analysis of the polymer layer mediated forces between colloids or star–star interactions [130–132]. Finally, all the above constitutes a first step toward the control of the dynamics in the linear regime. The much richer and more complex nonlinear dynamics represents a great challenge, some aspects of which are already being addressed [133–137].

Acknowledgments

This review was written when JR was a visiting scholar at FORTH during 2000–1, supported by a FORTH Fellowship. Fruitful collaboration on several aspects of the work presented in this review with the late G Fleischer, M Kapnistos, G Petekidis, R Seghrouchni, A N Semenov and G Vlachos is acknowledged with gratitude. Partial support was received from the EU (HPRN-CT-2000-00017), the Greek General Secretariat for Research and Technology (PLATON 1997–8) and the Greek Ministry of Education (applied molecular spectroscopy).

References

[1] McLeish T (ed) 1997 *Theoretical Challenges in the Dynamics of Complex Fluids* (*NATO ASI E339*) (Amsterdam: Kluwer)

[2] Cates M E and Evans M R (ed) 2000 *Soft and Fragile Matter: Nonequilibrium Dynamics Metastability and Flow* (Bristol: Institute of Physics Publishing)

[3] Muthukumar M, Ober C K and Thomas E L 1997 *Science* **277** 1225
[4] Likos C N 2001 *Phys. Rep.* **348** 267
[5] Vrij A and Philipse A P 1996 *Fine Particles Science and Technology* ed E Pelizzetti (Amsterdam: Kluwer)
[6] DeGennes P G 1996 *Fragile Objects: Soft Matter, Hard Science and the Thrill of Discovery* (New York: Springer)
[7] Witten T A 1999 *Rev. Mod. Phys.* **71** S367
[8] DeGennes P G 1979 *Scaling Concepts in Polymer Physics* (Ithaca, NY: Cornell University Press)
[9] Doi M and Edwards S F 1986 *The Theory of Polymer Dynamics* (New York: Oxford Science)
[10] Russel W B, Saville D A and Schowalter W R 1989 *Colloidal Dispersions* (New York: Cambridge University Press)
[11] Pusey P N and van Megen W 1986 *Nature* **320** 340
[12] Hamley I A, Daniel C, Mingvanish W, Mai S-M, Booth C, Messe L and Ryan A J 2000 *Langmuir* **16** 2508
[13] Hamley I W, Fairclough J P A, Ryan A J, Ryu C Y, Lodge T P, Gleeson A J and Pedersen J S 1998 *Macromolecules* **31** 1188
[14] Mortensen K 1992 *Europhys. Lett.* **19** 599
[15] Watanabe H 1997 *Acta Polym.* **48** 215
[16] Eiser E, Molino F and Porte G 2000 *Eur. J. Phys.* E **2** 39
[17] Lindenblatt G, Schärtl W, Pakula T and Schmidt M 2001 *Macromolecules* **34** 1730
[18] Gohr K, Pakula T, Tsutsumi K and Schärtl W 1999 *Macromolecules* **32** 7156
[19] Gast A P 1996 *Langmuir* **12** 4060
[20] Förster S, Wenz E and Lindner P 1996 *Phys. Rev. Lett.* **77** 95
[21] Buitenhuis J and Förster S 1997 *J. Chem. Phys.* **107** 262
[22] Sigel R *et al* 1999 *Phys. Rev. Lett.* **83** 4666
[23] Borrega R, Cloitre M, Betremieux I, Ernst B and Leibler L 1999 *Europhys. Lett.* **47** 729
[24] Cloitre M, Borrega R and Leibler L 2000 *Phys. Rev. Lett.* **85** 4819
[25] Castaing J C, Allain C, Auroy P, Auvray L and Pouchelon A 1996 *Europhys. Lett.* **36** 153
[26] Castaing J C, Allain C, Auroy P and Auvray L 1999 *Eur. J. Phys.* B **10** 61
[27] Nommensen P A, Duits M H G, Lopulissa J S, van den Ende D and Mellema J 1998 *Prog. Colloid Polym. Sci.* **110** 144
[28] Weiss A, Dingenouts N, Ballauff M, Senff H and Richtering W 1998 *Langmuir* **14** 5083
[29] Senff H, Richtering W, Norhausen C, Weiss A and Ballauff M 1999 *Langmuir* **15** 102
[30] Roovers J, Zhou L L, Toporowski P W, van der Zwan M, Iatrou H and Hadjichristidis N 1993 *Macromolecules* **26** 4324
[31] Zhou L L, Hadjichristidis N, Toporowski P M and Roovers J 1992 *Rubber Chem. Technol.* **65** 303
[32] Seghrouchni R, Petekidis G, Vlassopoulos D, Fytas G, Semenov A N, Roovers J J and Fleischer G 1998 *Europhys. Lett.* **42** 271
[33] Likos C N, Löwen H, Watzlawek M, Abbas B, Jucknischke O, Allgaier J and Richter D 1998 *Phys. Rev. Lett.* **80** 4450
[34] Toporowski P M and Roovers J 1986 *J. Polym. Sci., Part A: Polym. Chem. Ed.* **24** 3009
[35] Grest G S, Huang J S, Fetters L J and Richter D 1996 *Adv. Chem. Phys.* **XCIV** 67
[36] Daoud M and Cotton J B 1982 *J. Phys.* (*Paris*) **43** 831
[37] Birshtein T M and Zhulina E B 1984 *Polymer* **25** 1453
[38] Birshtein T M, Zhulina E B and Borisov O V 1986 *Polymer* **27** 1078
[39] Biver C, Hariharan R, Mays J and Russel W B 1997 *Macromolecules* **30** 1787
[40] Pakula T 1998 *Comp. Theor. Polym. Sci.* **8** 21
[41] Grest G S, Kremer K and Witten T A 1987 *Macromolecules* **20** 1376
[42] Willner L, Jucknischke O, Richter D, Roovers J, Zhou L -L, Toporowski P M, Fetters L J, Huang J S, Lin M Y and Hadjichristidis N 1994 *Macromolecules* **27** 3821
[43] Boothroyd A T and Ball R C 1990 *Macromolecules* **23** 1729
[44] Richter D, Jucknischke O, Willner L, Fetters L J, Lin M, Huang J S, Roovers J, Toporowski P M and Zhou L L 1993 *J. Phys.* (*Paris*) *IV Suppl.* C **8** 3
[45] Willner L, Jucknischke O, Richter D, Farago B, Fetters L J and Huang J S 1992 *Europhys. Lett.* **19** 297
[46] Ishizu K, Ono T and Uchida S 1997 *J. Colloid Interface Sci.* **192** 189
[47] Dozier W D, Huang J S and Fetters L J 1991 *Macromolecules* **24** 2810
[48] Grayce C J and Schweizer K S 1995 *Macromolecules* **28** 7461
[49] Witten T A, Pincus P A and Cates M E 1986 *Europhys. Lett.* **2** 137
[50] Vlassopoulos D, Pakula T, Fytas G, Roovers J, Karatasos K and Hadjichristidis N 1997 *Europhys. Lett.* **39** 617
[51] Semenov A N, Vlassopoulos D, Fytas G, Vlachos G, Fleischer G and Roovers J 1999 *Langmuir* **15** 358
[52] Huber K, Burchard W and Fetters L J 1984 *Macromolecules* **17** 541

[53] Roovers J, Toporowski P M and Douglas J 1995 *Macromolecules* **28** 7064
[54] Adam M, Fetters L J, Graessley W W and Witten T A 1991 *Macromolecules* **24** 2434
[55] Huber K, Bantle S, Burchard W and Fetters L J 1986 *Macromolecules* **19** 1404
[56] Merkle G, Burchard W, Lutz P, Freed K F and Gao J 1993 *Macromolecules* **26** 2736
[57] Pusey P N 1985 *Dynamic Light Scattering* ed R Pecora (New York: Plenum)
[58] Vlassopoulos D, Fytas G, Fleischer G, Pakula T and Roovers J 1999 *Faraday Discuss* **112** 225
[59] Sergè P N, Meeher S P, Pusey P N and Poon W C K 1995 *Phys. Rev. Lett.* **75** 958
[60] Sergè P N and Pusey P N 1996 *Phys. Rev. Lett.* **77** 771
[61] Grest G S, Kremer K, Milner S T and Witten T A 1989 *Macromolecules* **22** 1904
[62] Roovers J 1994 *Macromolecules* **27** 5359
[63] Vlassopoulos D, Fytas G, Pispas S and Hadjichristidis N 2001 *Physica* B **296** 184
[64] Mewis J, Frith W J, Strivens T A and Russel W B 1989 *AIChE J.* **35** 415
[65] Phan S, Russel W B, Cheng Z, Zhu J, Chaikin P M, Dunsmuir J H and Ottewill R H 1996 *Phys. Rev.* E **54** 6633
[66] Maranzano B J and Wagner N J 2000 *Rheol Acta* **39** 483
[67] Kärger J, Pfeifer H and Heink W 1988 *Adv. Magn. Res.* **12** 1
[68] Fleischer G, Fytas G, Vlassopoulos D and Roovers J 2000 *Physica* A **280** 266
[69] Vlachos G, Vlassopoulos D, Fytas G and Roovers J unpublished data
[70] Stellbrink J, Allgaier J and Richter D 1997 *Phys. Rev.* E **56** R3772
[71] Kapnistos M, Vlassopoulos D, Fytas G, Mortensen K, Fleischer G and Roovers J 2000 *Phys. Rev. Lett.* **85** 4072
[72] Pakula T, Vlassopoulos D, Fytas G and Roovers J 1998 *Macromolecules* **31** 8931
[73] Hatzikiriakos S G, Kapnistos M, Vlassopoulos D, Chevillard C, Winter H H and Roovers J 2000 *Rheol. Acta* **39** 38
[74] Ferry J D 1980 *Viscoelastic Properties of Polymers* (New York: Wiley)
[75] Fetters L J, Kiss A D, Pearson D S, Quack G F and Vitus F J 1993 *Macromolecules* **26** 4324
[76] Pakula T, Geyler S, Edling T and Boese D 1996 *Rheol. Acta* **35** 631
[77] Kremer F, Boese D and Fetters L 1991 *J. Non-Cryst. Solids* **131–133** 728
[78] Milner S T and McLeish T C B 1997 *Macromolecules* **30** 2159
[79] McLeish T C B and Milner S T 1999 *Adv. Polym. Sci.* **143** 195
[80] Milner S T and McLeish T C B 1998 *Macromolecules* **31** 7479
[81] Kapnistos M, Semenov A N, Vlassopoulos D and Roovers J 1999 *J. Chem. Phys.* **111** 1753
[82] Ball R C and McLeish T C B 1989 *Macromolecules* **22** 1911
[83] Pakula T 1996 *J. Computer-Aided Mat. Des.* **3** 351
[84] Pakula T and Teichmann J 1997 *Mater. Res. Soc. Symp. Proc.* **455** 211
[85] Vlassopoulos D, Fytas G, Loppinet B, Isel F, Lutz P and Benoit H 2000 *Macromolecules* **33** 5960
[86] Graessley W W and Roovers J 1979 *Macromolecules* **12** 959
[87] Roovers J 1985 *Polymer* **26** 1091
[88] Watzlawek M, Likos C N and Löwen H 1999 *Phys. Rev. Lett.* **82** 5289
[89] Löwen H, Watzlawek M, Likos C N, Schmidt M, Jusufi A and Denton A R 2000 *J. Phys.: Condens. Matter* **12** A465
[90] Watanabe H, Kanaya T and Takahashi Y 2001 *Macromolecules* **34** 662
[91] McConnel G A and Gast A P 1997 *Macromolecules* **30** 435
[92] Pakula T 2000 *J. Mol. Liquids* **86** 109
[93] Roovers J 1991 *Macromolecules* **24** 5895
[94] Watanabe H, Sato T, Osaki K, Hamersky M W, Chapman B R and Lodge T P 1998 *Macromolecules* **31** 3740
[95] Roovers J, Toporowski P and Martin J 1989 *Macromolecules* **22** 1897
[96] Loppinet B, Stiakakis E, Vlassopoulos D, Fytas G and Roovers J 2001 *Macromolecules* at press
[97] Tsukahara Y, Namba S-I, Iwasa J, Nakano Y, Kaeriyama K and Takahashi M 2001 *Macromolecules* **34** 2624
[98] Gerle M, Fischer K, Roos S, Müller A H E, Schmidt M, Sheiko S S, Prokhorova S and Möller M 1999 *Macromolecules* **32** 2629
[99] Vlassopoulos D, Pakula T, Fytas G, Pitsikalis M and Hadjichristidis N 1999 *J. Chem. Phys* **111** 1760
[100] Vlassopoulos D, Pitsikalis M and Hadjichristidis N 2000 *Macromolecules* **33** 9740
[101] Pham Q T, Thibeault J C, Lau W and Russel W B 1999 *Macromolecules* **32** 2996
[102] Pham Q T, Russel W B, Thibeault J C and Lau W 1999 *J. Rheol.* **43** 1599
[103] Séréto Y, Aznar R, Porte G, Berret J -F, Calvet D, Collet A and Viguier M 1998 *Phys. Rev. Lett* **81** 5584
[104] Knauss D M, Al-Muallem H, Huang T and Wu D T 2000 *Macromolecules* **33** 3557
[105] Simon P F W, Müller A H E and Pakula T 2001 *Macromolecules* **34** 1677
[106] Brunsveld L, Folmer J B and Meijer E W 2000 *MRS Bull.* **25** 49
[107] Likos C N, Schmidt M, Löwen H, Balauff M, Pötschke D and Lindner P 2001 *Macromolecules* **34** 2914
[108] Baars M W P L, Karlsson A J, Sorokin V, deWaal B F W and Meijer E W 2000 *Angew. Chem. Int. Ed.* **39** 4262

[109] Guo X, Weiss A and Ballauff M 1999 *Macromolecules* **32** 6043
[110] Hariharan R, Biver C, Mays J and Russel W B 1998 *Macromolecules* **31** 7506
[111] Batra U, Russel W B, Pitsikalis M, Sioula S, Mays J W and Huang J S 1997 *Macromolecules* **30** 6120
[112] Halperin A, Tirrell M and Lodge T P 1992 *Adv. Polym. Sci.* **100** 31
[113] Loppinet B, Sigel R, Larsen A, Fytas G, Vlassopoulos D and Liu G 2000 *Langmuir* **16** 6480
[114] Mecerreyes D, Lee V, Hawker C J, Hedrick J L, Wursch A, Volksen W, Magbitang T, Huang E and Miller R D 2001 *Adv. Mater.* **13** 204
[115] Roovers J and Graessley W W 1981 *Macromolecules* **14** 766
[116] Struglinski M J, Graessley W W and Fetters L J 1988 *Macromolecules* **21** 783
[117] Roovers J 1987 *Macromolecules* **20** 148
[118] Milner S T, McLeish T C B, Young R N, Hakiki A and Johnson J M 1998 *Macromolecules* **31** 9345
[119] Blottière B, McLeish T C B, Hakiki A, Young R N and Milner S T 1998 *Macromolecules* **31** 9295
[120] Halperin A and Alexander S 1988 *Europhys. Lett.* **6** 329
[121] Raphaël E, Pincus P and Fredrickson G H 1993 *Macromolecules* **26** 1996
[122] Poon W C K, Pirie A D and Pusey P N 1995 *Faraday Disc.* **101** 65
[123] Poon W C K 1998 *Curr. Opin. Colloid Interface Sci.* **3** 593
[124] Dzubiella J, Jusufi A, Likos C N, von Ferber C, Löwen H, Stellbrink J, Allgaier J, Richter D, Schofield A B, Smith P A, Poon W C K and Pusey P N 2001 *Phys. Rev.* E **64** R104
[125] Hilliou L, Vlassopoulos D and Rehahn M 2001 *Macromolecules* **34** 1742
[126] Bockstaller M, Köhler W, Wegner G, Vlassopoulos D and Fytas G 2000 *Macromolecules* **33** 3951
[127] Pakula T and Harre K 2000 *Comp. Theor. Polym. Sci.* **10** 197
[128] Blackwell R J, Harlen O G and McLeish T C B 2001 *Macromolecules* **34** 2579
[129] McLeish T C B and Larson R G 1998 *J. Rheol.* **42** 81
[130] Chatterjee A P and Schweizer K S 1998 *J. Chem. Phys.* **109** 10464
[131] Fuchs M and Schweizer K S 2000 *Europhys. Lett.* **51** 621
[132] vonFerber C, Jusufi A, Walzlawek M, Likos C N and Löwen H 2000 *Phys. Rev.* E **62** 6949
[133] Archer L A and Varshney S K 1998 *Macromolecules* **31** 6348
[134] Mhetar V and Archer L A 1999 *J. Non-Newton. Fluid Mech.* **81** 71
[135] Watanabe H 1999 *J. Non-Newton. Fluid Mech.* **82** 315
[136] Marrucci G, Greco F and Ianniruberto G 1999 *Curr. Opin. Colloid Interface Sci.* **4** 283
[137] Marrucci G 1996 *J. Non-Newton. Fluid Mech.* **62** 279